Measurement: Sensors 38 (2025) 101423

Contents lists available at ScienceDirect

Measurement: Sensors

journal homepage: www.sciencedirect.com/journal/measurement-sensors

Development and calibration of a measurement system for the characterization of avalanche photodiodes prospectively used as sensors in X-ray Compton polarimeters for space

ARTICLE INFO

Keywords:
X-ray polarimeter
Avalanche photodiode
Measurement system for APD calibration

ABSTRACT

Solar flares, dynamic eruptions of electromagnetic radiation from the Sun's surface, represent a potential risk for various human technological infrastructures. The CUbesat Solar Polarimeter (CUSP) project, part of the Alcor Program of the Italian Space Agency, aims to measure solar flare polarization in the hard X-ray band. This paper focuses on the design and setup of a measurement system to characterize the response of the avalanche photodiodes (APD) used in the CUSP polarimeter. The system is tested at room temperature conditions by varying both incident photon energy between 20 keV and 135 keV, using X-ray sources as references, and APD bias voltage from 260 V to 410 V. Using the calibrated system, the dependence of APD gain on bias voltage, and its energy resolution, are measured, matching the metrological standards of the polarimeter.

1. Introduction

Solar flares (SFs), powerful bursts of electromagnetic radiation originating from the Sun surface, are highly energetic phenomena emitting in a wide range of electromagnetic radiation, including X-rays. SFs represent dynamic events within the Sun's atmosphere, showcasing its complex and dynamic nature [1,2]. The consequences of SFs on human activities can be relevant. While the Earth atmosphere provides a shield against most of the solar radiation, energetic flares can still impact various technological systems. For instance, disruptions in satellite communications, power grids, and even GPS systems have been observed during periods of heightened solar activity. Understanding the mechanisms behind solar flares and their potential impact is therefore of great importance for safeguarding our technological infrastructure [3–6].

In recent years, there has been a growing emphasis on the development of innovative measurement techniques for studying solar flares, including polarimetry of X-rays [2,7]. The CUbesat Solar Polarimeter (CUSP) project [8] is a CubeSat mission currently under development in the framework of the Alcor Program of the Italian Space Agency that will start Phase B in 2024. The aim of this mission is the measurement of the linear polarization of solar flares in the hard X-ray band to predict the risk posed by the arrival of charged particle clouds on Earth and act preventively to secure sensitive systems [8].

The payload of CUSP is made up of an X-ray Compton polarimeter composed of plastic and inorganic scintillators. The light emitted by the interaction of the X-ray radiation with the scintillators is read by multianode photomultiplier tubes (MAPMT) in time coincidence with an array of 32 avalanche photodiodes (APDs). An accurate characterization of the response of the used APDs in terms of gain G_{APD} and energy resolution, is therefore fundamental to meet the target metrological characteristics of the whole polarimeter [8]. In this work, we present the design and set-up of a measurement system able to characterize the response of the APDs when the energy E of the impinging photons and the bias voltage V_b are changed. ^{55}Fe, ^{109}Cd, ^{241}Am, and ^{57}Co radioactive samples were used as reference photon sources and placed both in direct contact with the APD and interposing between these the $Gd_3Al_2Ga_3O_{12}$ (GAGG) inorganic scintillator [9] that will be used in the final configuration of the polarimeter. Whereas the response of the APD was calibrated changing V_b between 260 V and 410 V.

The paper is organized as follows: in Sec. 1 the measurement system and procedure are described, in Sec. 2 the calibration of the system and results on the characterization of the used APD are discussed. Finally, in Sec. 3 conclusions are given.

2. Measurement system and procedures

Avalanche photodiodes (APDs) are semiconductor devices used for detecting and amplifying low-level radiations. These photodiodes are designed to operate in the reverse bias mode, where a high voltage V_{bias} is applied across the device to create a strong electric field within the depletion zone. This electric field accelerates charge carriers (electrons and holes) generated by incident photons, leading to a phenomenon known as avalanche multiplication, thus to an overall charge gain [10,11].

The gain G_{APD} of an APD is defined as

$$G_{APD} = (I_D - I_{ds}) \,/\, I_{dg} \approx I_D \,/\, I_{dg}, \tag{1}$$

where I_D is the total dark current of the diode, I_{ds} is the surface leakage current and I_{dg} is the bulk generated current inside the APD substrate. Since G_{APD} is determined by the ionization rate, and this in turn is determined by the electric field across the depletion zone, i.e. by the reverse bias voltage V_{bias} applied [10,11], then $G_{APD} = f(V_{bias})$ with $f(\cdot)$ being the calibration function that needs to be known and that, with the system here implemented, we aim to determine. It is worth noting that the so defined G_{APD} is defined on the multiplication of charge in the

https://doi.org/10.1016/j.measen.2024.101423

Available online 21 December 2024

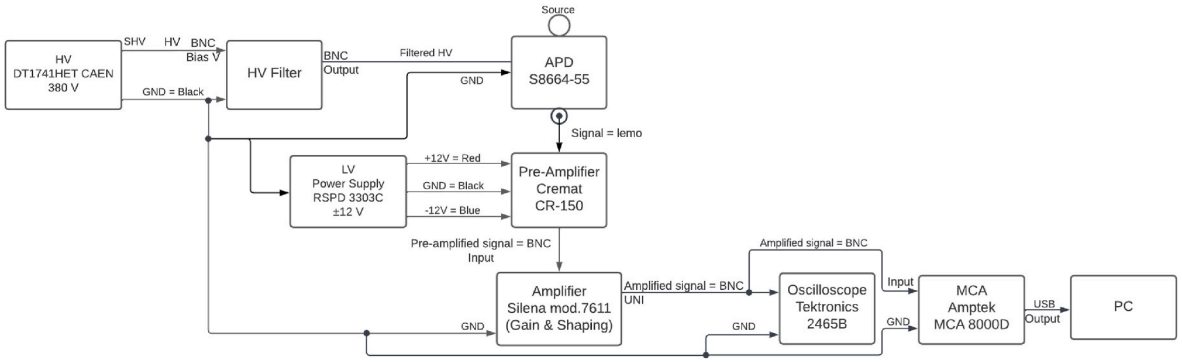

Fig. 1. Block diagram of the measurement system.

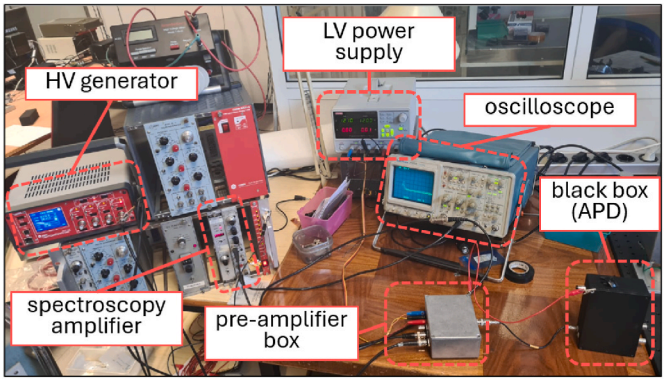

Fig. 2. Picture of the developed measurement set-up.

depletion zone, hence it does not include frequency dependent phenomena as the quantum efficiency of the device. We note also that G_{APD} depends on the operational temperature. We defer to a future experimental study the development of the present method and system for the temperature-dependent calibration.

The other figure of merit in APDs used in spectroscopy applications is their energy E resolution $\delta E/E$ [12]. This depends on the quantum fluctuations in the avalanche charge generation process and in the noise, hence also on V_{bias} itself.

We now turn to the description of the system able to characterize the aforementioned quantities as a function of V_{bias} and the energy of the impinging photons.

2.1. The measurement system

The block diagram of the measurement system is shown in Fig. 1 and a picture shown in Fig. 2. It is composed by a High Voltage (HV) source DT1471HET CAEN which is used to generate V_{bias}. The output of the HV source is not directly applied to the APD but first filtered by the capacitive filter mounted on the Cremat CR-150 evaluation board. The filter resistance can be regulated by the user depending on the APD dark current.

The so biased APD is mounted into a black shielded box (in order to avoid the absorption of external photons) and illuminated with the selected radiation sources. The charge pulses generated by the APD are conditioned by the Cremat CR-110R2.2 charge preamplifier mounted on the CR-150 evaluation board. Each charge pulse is integrated by the preamplifier thus obtaining as the output a voltage pulse whose magnitude is proportional to the total charge in the originating charge pulse. The preamplifier conversion factor is 1.4 V/pC. The feedback resistor $R_f \approx 100\ \mathrm{M}\Omega$ placed in parallel to the feedback capacitor $C_f \approx 1.4$ pF in the preamplifier loop produces an exponential time decay of each pulse with characteristic time $\tau \approx 140\ \mu$s. This theoretically limits the pulses duration accepted by the preamplification input in order to avoid output distortions given by the pile-up of several pulses. Due to the Poisson statistics of emitting sources, it is not possible to avoid this phenomenon. For this reason, pulse shaping stages are usually used in these situations [13]. The shaping of exponentially decaying voltage pulses into sinc or gaussian pulses alleviates the pile-up problem, but to avoid losing information about the input charge pulses, it is necessary for the amplitude of the shaped-pulses to be proportional to the amplitude of the output pulses from the charge preamplifier, despite their different temporal extent. The pulse shaping operation and amplitude amplification is performed with the Silena 7611 spectroscopy amplifier. The used Silena amplifier allows for a continuous gain regulation from 2.5 to 3000, with thermal stability of ± 50 ppm/°C, and it is based on a Gaussian filter dedicated to the pulse-shaping stage with variable shaping time t_s from 0.25 μs to 6 μs.

Finally, a multi-channel analyser (MCA) is used as analog to digital conversion stage to count the number of received pulses and to classify these on their voltage amplitude. MCA are commonly used in spectroscopy to analyse the energy distribution of incoming radiation. This instrument consists of a series of channels, each corresponding to a specific energy range, into which detected radiation events are sorted based on their energy levels. The MCA, when used in the pulse-height analysis mode, then records the number of events detected in each channel, producing a histogram or spectrum that represents the energy distribution of the incoming radiation. The Amptek MCA8000D is used in this measurement set-up. The conversion time of this MCA is 10 ns, thus negligible with respect to the signal to be analysed.

An oscilloscope is therefore used to allow the user to visualize the pulses shape from the pulse shaper and to assess the proper operation and settings of all instruments employed.

Measuring the gain of the APD, and consequently experimentally evaluating the calibration curve $G_{APD} = f(V_{bias})$, is carried out by measuring the amplitude of the voltage pulses in input to the MCA. The analytical evaluation of the amount of charge generated by the APD for each received photon requires a precise understanding of the amplification introduced by each stage of the measurement system and an accurate knowledge of the attenuations introduced by the cables and connectors used. Therefore, calibrating the measurement system itself, taking into account the effect that each component has on the signal amplitude, is not only complex but also inevitably leads to unacceptable uncertainties if performed with standard laboratory instruments. The simplest and most economical way would be to employ a calibrated reference for generating charge/current pulses to input into the measurement system. For this reason, to calibrate the system, it was decided to use an APD whose gain, under specific operating conditions, is known. In this case, the Si S8664-55 Hamamatsu photodiode [14], serial number AA4400, was used. Its breakdown voltage is $V_b \approx 433$ V, and its gain is $G_{APD,ref} = 50 \pm 1$ at ~ 25 °C, with $V_{bias} = (382.3 \pm 0.1)$ V, where the number following the symbol $\pm$ is to be read as the numerical value of an extended uncertainty with 100 % probability level based on a

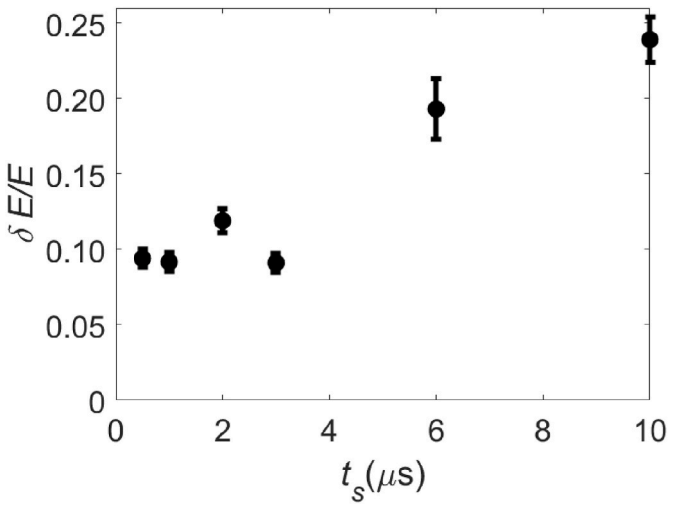

Fig. 3. Energy resolution $\frac{\delta E}{E}$ measurements for different settings of the shaping time t_s. Data are measured placing the ^{55}Fe sample directly illuminating the APD.

uniform distribution [15]. The uncertainty on the reference gain value provided by the producer is not limiting for the final application of the APD in the X-ray polarimeter, thus the use of this value as reference is justified.

2.2. The measurement procedure

The measurements were performed placing different radioactive sources with the following configurations:

- ^{55}Fe, directly illuminating the APD;
- ^{109}Cd + GAGG scintillator;
- ^{241}Am + GAGG scintillator;
- ^{57}Co + GAGG scintillator.

The histograms collected by the MCA are then fitted with a gaussian function. The width of the experimental distribution to be fitted with the gaussian model is determined minimizing the χ^2 value, that is finding the portion of the peak that is most close to that of a gaussian distribution. From the fitting procedure the peak position Ch_{pk} and the standard deviation σ_{pk} are measured. Standard uncertainties $u(Ch_{pk})$ and $u(\sigma_{pk})$ are evaluated by the covariance matrix given by the least-square fitting method [16]. From Ch_{pk} and σ_{pk} the energy resolution is obtained as follows:

$$\frac{\delta E}{E} = \frac{FWHM}{Ch_{pk}} = 2.35\frac{\sigma_{pk}}{Ch_{pk}} \ . \tag{2}$$

3. Results and discussion

Before proceeding with the use of the implemented system, it is necessary to evaluate and properly set the gain and shaping time t_s of the amplification stage. To this aim, the ^{55}Fe source was positioned directly on the APD. By biasing the APD with $V_{bias} = 380$ V, the effect of employing different shaping times on $\frac{\delta E}{E}$ of the system was evaluated. To ensure that the overall energy resolution of the system is not dependent on t_s, thus masking the resolution of the APD to be characterized, t_s was adjusted by lowering it until its effect on the measured energy resolution was negligible. From the plot shown in Fig. 3, it can be seen that for $t_s >$ 3 μs, the measured $\delta E/_E$ begins to increase drastically, indicating the introduction of an effect of the measurement system itself on the overall resolution. For this reason, all subsequent measurements were performed with $t_s = 1$ μs.

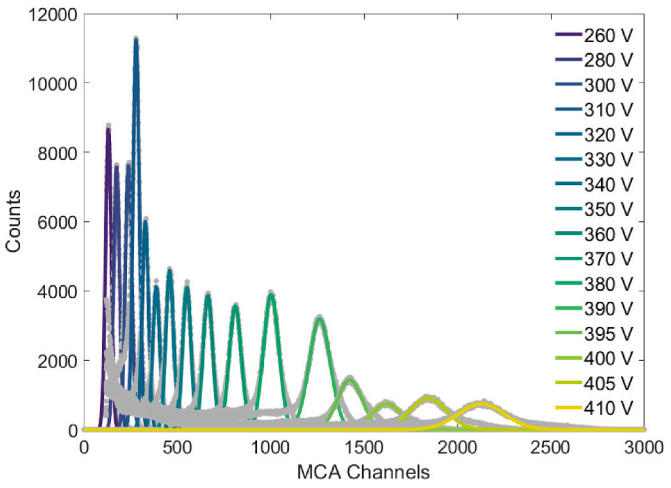

Fig. 4. Output of the MCA when the APD under test is biased at different V_{bias}. Data are measured placing the ^{55}Fe sample directly illuminating the APD.

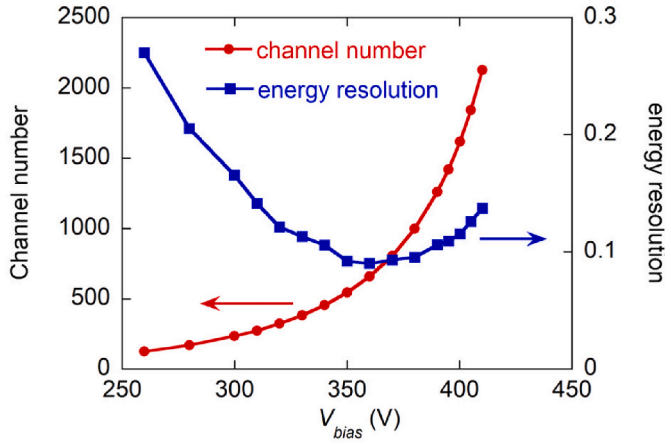

Fig. 5. Position, in terms of the channel number of the MCA, of the centroid of the gaussian distributions measured by the MCA (red points – left scale) for different V_{bias} values. Energy resolution as a function of V_{bias} (blue squares – right scale). Data are measured placing the ^{55}Fe sample directly illuminating the APD. Lines are guides for the eye.

Once the measurement system is correctly set, the effect of the direct irradiation of the APD with the ^{55}Fe source is evaluated. During the test, the APD V_{bias} is changed from 260 V to 410 V. Due to the sensitivity of G_{APD} to V_{bias}, when V_{bias} is increased the position of Ch_{pk} is expected to increase due to the larger amount of charges generated by the avalanche phenomenon. The result is shown in Fig. 4.

From the fit of the data shown in Fig. 4 with the procedure discussed in Section 1.2, the peak position Ch_{pk} and the energy resolution are evaluated as a function of V_{bias}. The result is shown in Fig. 5.

The experimentally measured $\delta E/_E(V_{bias})$ shows a minimum at 350 V $< V_{bias} <$ 380 V. For these V_{bias} values $\delta E/_E < 0.10$. Thus, we decided to bias the APD at 360 V in order to work in the lowest $\delta E/_E$ region. In addition to this, from the data shown in Fig. 4, it was possible to determine the calibration curve $G_{APD} = f(V_{bias})$. For the used APD $G_{APD}(382.3\ \text{V}) = G_{APD,ref}$ (from the calibration provided by the producer), thus by interpolating the data shown in Fig. 5 the MCA channel corresponding to this V_{bias} value can be determined $Ch_{Gref} = 1052 \pm 1$. Exploiting the linearity of the MCA output the following calibration curve for the MCA channels Ch_{MCA} can be obtained:

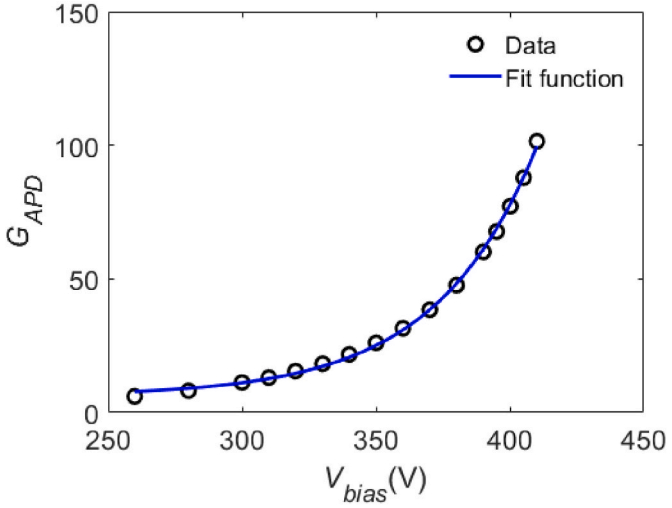

Fig. 6. Determination of the calibration curve $G_{APD}(V_{bias})$. Data are measured placing the ^{55}Fe sample directly illuminating the APD. Uncertainty bars are contained in the symbols dimension.

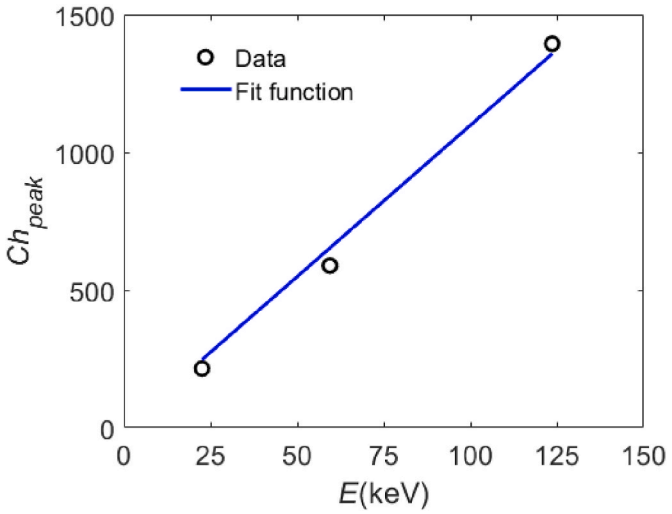

Fig. 7. Energy calibration curve of the developed system. The position of the centroids, in terms of the channel number of the MCA, with respect to the energy of the incident X-ray photons. Data are measured using the ^{109}Cd, ^{241}Am, ^{57}Co samples with GAGG. Uncertainty bars are contained in the symbols dimension.

$$G_{APD} = \frac{Ch_{MCA} G_{APD,ref}}{Ch_{Gref}}. \tag{3}$$

With Eq. (3) the plot shown in Fig. 6 is obtained. This is best fitted with the following exponential function:

$$G_{APD} = a + be^{c\ V_{Bias}}, \tag{4}$$

with $a = 6.0$, $b = 1.8 \times 10^{-4}$, $c = 2.65 \times 10^{-4}$ V^{-1} and the covariance matrix:

$$U_G = = \begin{bmatrix} 0.55 & -3.3 \times 10^{-4} & 4.5 \times 10^{-4}\ \mathrm{V}^{-1} \\ -3.3 \times 10^{-4} & 2.8 \times 10^{-7} & -3.8 \times 10^{-7}\ \mathrm{V}^{-1} \\ 4.5 \times 10^{-4}\ \mathrm{V}^{-1} & -3.8 \times 10^{-7}\ \mathrm{V}^{-1} & 5.3 \times 10^{-7}\ \mathrm{V}^{-2} \end{bmatrix}. \tag{5}$$

The energy calibration of the measurement system is finally performed using different radioactive sources, coupled with the APD through the GAGG scintillator, thus in the final configuration composed by APD and scintillator. This is needed to associate the MCA ADC channels to the irradiating energy photons, once V_{bias} is kept fixed. The sources are placed on the external of the APD black box in which a small hole is performed, and then covered with black isolating tape, to allow the passage of the X-ray radiation through the hole itself while blocking external lower frequencies photons. Finally, the sources are covered with a tungsten cap to protect the user from X-ray irradiation. In all the following measurements the reference APD is biased with $V_{bias} = 380$ V and the Silena 7611 gain is set at 210, with $t_s = 1\ \mu$s.

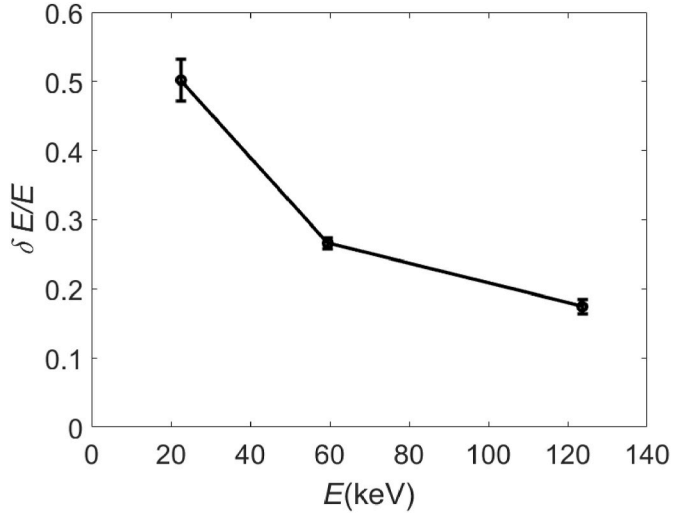

Fig. 8. Energy resolution as a function of the energy of the incident X-ray photons. Data are measured using the ^{109}Cd, ^{241}Am, ^{57}Co samples with GAGG. Lines are guides for the eye.

Since the X-ray photons emitted from the different sources have different energies, it is possible to associate to Ch_{pk} the values of the energy emission lines of the used sources. In particular, ^{109}Cd emission is mainly at 22 keV and 25 keV. Due to the limited energy resolution of the APD these are not resolved, and these lines are seen as a unique peak corresponding to 22.6 keV. The ^{241}Am line of interest is at 59.5 keV. The ^{57}Co emits on different lines from 122 keV to 136 keV, with an average value at 123.55 keV.

The light yield of GAGG crystal is about 50 photons/keV and the scintillation occurs in the optical band, peaking at 520 nm [9]. The linear dependence of the number of photons emitted in the GAGG crystal with respect to the energy of the absorbed X-ray photon is exploited to find the relationship between the channel number of the MCA and the photon energy of the photons (since this is proportional to the voltage of the shaped pulses). The result is shown in Fig. 7.

The experimental data shown in Fig. 7 are fitted with the linear function $Ch_{peak} = mE$, with $m = 10.9(8)$ keV^{-1}, where the number in parentheses is the numerical value of the standard uncertainty expressed in the unit of the quoted result [15].

Finally, the energy resolution measured with the different radioactive sources is shown as a function of the incident X-ray photons in Fig. 8.

4. Conclusions

A measurement system able to characterize the gain and energy resolution of APDs prospectively used in a space X-ray polarimeter was described in the paper. The system allows to collect the charge pulses generated by the APD when properly irradiated. These are converted and shaped in voltage pulses which are finally measured by a MCA working in the in the pulse-height analysis mode.

The attenuations and gain introduced by the system are calibrated using as reference an APD whose gain, in determined conditions, is known. Whereas the calibration of the system in energy of the incident photons in the X-ray band was performed using as references samples of radioactive materials.

The so calibrated system was finally tested on a specific APD to obtain the gain-bias voltage calibration curve and to assess the energy resolution of the APD. The results demonstrate the applicability of the developed system to the characterization of the APDs of interest in this study.

The results here shown were obtained at room temperature. Future work will extend the APD calibration to the wider temperature range where the APD are expected to operate when mounted in the payload of the CUSP mission [17,18]. Finally, once the measurement system will be defined and set-up to operate in a climate chamber, the metrological traceability chain will be identified, and the system used to characterize the arrays of APD that will be mounted in the CubeSat constellation.

Funding statement

Activity funded by ASI-INAF CUSP phase A contract 2022-4-R.0.

References

[1] E. Tandberg-Hanssen, A. Gordon Emslie, The Physics of Solar Flares, vol. 14, Cambridge University Press, 1988.
[2] L. Fletcher, B.R. Dennis, H.S. Hudson, S. Krucker, K. Phillips, A. Veronig, M. Battaglia, L. Bone, A. Caspi, Q. Chen, P. Gallagher, P.T. Grigis, H. Ji, W. Liu, R. O. Milligan, M. Temmer, An observational overview of solar flares, Space Sci. Rev. 159 (2011) art. id 19.
[3] R.J. McAteer, P.T. Gallagher, P.A. Conlon, Turbulence, complexity, and solar flares, Adv. Space Res. 45 (9) (2010) 1067–1074.
[4] J.A. Joselyn, The impact of solar flares and magnetic storms on humans, Eos, Trans. Am. Geophys. Union 73 (7) (1992) 81–85.
[5] E.L. Afraimovich, G.A. Zherebtsov, G. Ya Smol'Kov, Total failure of GPS during a solar flare on December 6, 2006, Dokl. Earth Sci. 417 (1) (2007) 1231–1235.
[6] J.A. Joselyn, The human impact of solar flares and magnetic storms, in: From the Sun: Auroras, Magnetic Storms, Solar Flares, Cosmic Rays, American Geophysical Union, Washington DC, 1998, pp. 67–72.
[7] S. Fabiani, Instrumentation and future missions in the upcoming era of X-ray polarimetry, Galaxies 6 (2) (2018) 54.
[8] S. Fabiani, et al., CUSP: a two CubeSats constellation for space weather and solar flares x-ray polarimetry, in: Space Telescopes and Instrumentation 2022: Ultraviolet to Gamma Ray., SPIE 12181, 2022, pp. 106–114.
[9] M. Yoneyama, J. Kataoka, M. Arimoto, T. Masuda, M. Yoshino, K. Kamada, A. Yoshikawa, H. Sato, Y. Usuki, Evaluation of GAGG:Ce scintillators for future space applications, J. Instrum. 13 (2018) P02023.
[10] A. Sedra, K.C. Smith, T.C. Carusone, V. Gaudet, in: Microelectronic circuits 8th edition, the oxford series in electrical and computer engineering, 2020.
[11] M.J.N. Sibley, Photodiodes, Optical Communications: Components and Systems, Springer Link, 1995, pp. 153–181.
[12] B.K. Agarwal, X-Ray Spectroscopy: an Introduction, Springer, 2013.
[13] W.R. Leo, Techniques for Nuclear and Particle Physics Experiments: a How-To Approach, Springer Science & Business Media, 2012.
[14] T. Ikagawa, Performance of large-area avalanche photodiode for low-energy X-rays and γ-rays scintillation detection, Nucl. Instrum. Methods Phys. Res. Sect. A Accel. Spectrom. Detect. Assoc. Equip. 515 (3) (2003) 671–679.
[15] Joint Committee for Guides in Metrology (JCGM), JCGM 100:2008 Evaluation of measurement data- Guide to the expression of uncertainty in measurement, JCGM (2008).
[16] Joint Committee for Guides in Metrology (JCGM), JCGM 102:2011 Evaluation of measurement data- Supplement 2 to the "Guide to the expression of uncertainty in measurement" – extension to any number of output quantities, JCGM (2011).
[17] A. Alimenti, et al., Design and test of a calibration system for avalanche photodiodes used in X-ray Compton polarimeters for space, Sensors 24 (2024) 8016.
[18] F. Cologgi, et al., Characterization of avalanche photodiodes (APDs) for the CUbesat Solar Polarimeter (CUSP) mission, in: Space Telescopes and Instrumentation 2024: Ultraviolet to Gamma Ray 13093, 2024, pp. 2241–2244.

A. Alimenti[a,*], F. Cologgi[a], E. Silva[a], S. Fabiani[b,**], A. Rubini[b], P. Loffredo[b], G. Lombardi[b], P. Soffitta[b], E. Del Monte[b], E. Costa[b], N. De Angelis[b], S. Di Cosimo[b], F. Muleri[b], A. Di Marco[b], A. Terracciano[c], E. Zaccagnino[c], I. Donnarumma[c], D. Brienza[c], G. Leccese[c], A. Fedele[c], S. Natalucci[c], G. Cucinella[d], A. Negri[d], S. Bonomo[d], S. Di Filippo[d], M. Perelli[d], D. Modenini[e], A. Curatolo[e], A. Locarini[e], P. Tortora[e], I. Baffo[f], P. Fanelli[f], A. Del Re[g], G. De Iulis[g], P. Leonetti[g], A. Zambardi[g], G. De Cesare[h], R. Campana[h], M. Centrone[i], G. Minervini[j]

[a] *Dept. of Industrial, Electronic and Mechanical Engineering, Roma Tre University, Via V. Volterra 62, 00146, Rome, Italy*
[b] *INAF-IAPS, via del Fosso del Cavaliere 100, 00133, Rome, Italy*
[c] *Agenzia Spaziale Italiana, via del Politecnico snc, 00133, Rome, Italy*
[d] *IMT s.r.l., via Carlo Bartolomeo Piazza 30, 00161, Rome, Italy*
[e] *Dept. of Industrial Engineering and Interdepartmental Center for Industrial Aerospace Research, Alma Mater Studiorum Università di Bologna, Via Fontanelle 40, 47121, Forlí, Italy*
[f] *DEIM, Università degli studi della Tuscia, Largo dell'Università, 01100, Viterbo, Italy*
[g] *SCAI Connect s.r.l., Via Vincenzo Lamaro 51, 00173, Roma, Italy*
[h] *Dip. di Ingegneria dell'Impresa «Mario Lucenti», Università degli Studi di Roma "Tor Vergata", Via Cracovia 50, 00133, Roma, Italy*
[i] *INAF-OAR, Via Frascati 33, 00040, Monte Porzio Catone, Italy*
[j] *INAF Headquarters, Viale del Parco Mellini 84, 00136, Roma, Italy*

[*] Corresponding author.

[**] Corresponding author.
E-mail addresses: andrea.alimenti@uniroma3.it (A. Alimenti), sergio.fabiani@inaf.it (S. Fabiani).